Dry Metal Forming Open Access Journal

Fast Manuscript Track

Edited by Frank Vollertsen
Available online at elib.suub.uni-bremen.de

www.drymetalforming.de

Dry Met. Forming OAJ FMT 1 (2015) 121–133
Received 25 September 2015; published 04 November 2015

Development and Evaluation of Tool Sided Surface Modifications for Dry Deep Drawing of Steel and Aluminum Alloys

Marion Merklein[1], Michael Schmidt[2], Sandro Wartzack[3], Stephan Tremmel[3], Kolja Andreas[1], Tom Häfner[2], Rong Zhao[3], Jennifer Steiner[1]*

[1]Institute of Manufacturing Technology, Friedrich-Alexander-Universität Erlangen-Nürnberg, Egerlandstr. 13, 91058 Erlangen, Germany
[2]Institute of Photonic Technologies, Friedrich-Alexander-Universität Erlangen-Nürnberg, Konrad-Zuse-Str. 3/5, 91052 Erlangen, Germany
[3]Institute of Engineering Design, Friedrich-Alexander-Universität Erlangen-Nürnberg, Martensstr. 9, 91058 Erlangen, Germany

Abstract

Avoiding negative effects of conventional lubrication in forming operations stimulates research on lubricant free forming processes. Increased friction and wear due to direct contact between tool and workpiece surface lead to insufficient forming results in dry forming operations. Dry deep drawing of rectangular cups with conventional tools reveals cracks and wrinkles. This necessitates the development of tool sided surface modifications which face the challenges of lubricant free forming. As former results of tribological investigations have shown, adhesion is the dominant friction and wear mechanism. Therefore, diamond-like carbon coatings are applied to decrease adhesion. The mechanical properties of a-C:H:W- and ta-C-coatings are systematically analyzed to reduce friction and wear. Additionally, micro features are generated by laser texturing of a-C:H:W coatings to control material flow by locally adapted frictional conditions. The effects of different feature edge geometries and the feature orientation are investigated in ring-on-disc tribometer tests. Depending on the deposition parameters some a-C:H:W coating variants show reduction of adhesion for DC04. However, in contact with aluminum alloys no improve of tribological conditions could be achieved. ta-C coatings affect the reduction of friction and wear in contact with DC04 and aluminum and show high potential for application in dry forming processes. Depending on adhesion affinity of the workpiece material, micro features can increase friction by adjusting their edge geometry, orientation and area coverage. The tribological behavior of selected surface modifications is finally analyzed in the strip drawing test. The obtained results gain basic knowledge for development of surface modifications towards realization of lubricant free deep drawing by a tailored tool concept.

Keywords: Dry Deep Drawing, Tribology, Laser Generated Micro Features, Carbon Based Coatings

1 Introduction

Due to high material utilization, sheet metal forming processes belong to energy efficient production technologies. However, there is still potential for further increase in resource efficiency. In conventional sheet metal forming operations lubricants are applied to decrease friction and increase tool life as well as workpiece quality. Most lubricants are made of non-renewable resources and contain health-damaging, environmental harmful ingredients like chloroparaffins [1]. Thus, high effort is needed for a proper disposal of these lubricants. After the forming process, the workpiece needs an intensive cleaning and drying before further production steps like varnishing or welding can be proceeded. These negative impacts of conventional lubrication motivate the realization of dry forming processes which is the goal of the DFG priority program SPP1676. According to Vollertsen et al. [2] dry forming is achieved when the workpiece leaves the tool without the necessity of cleaning and drying. Encouraged by the ecological and economical potentials of dry forming, the scope of this research project is the realization of lubricant free deep drawing. The results of a dry deep drawing operation with conventional tooling concepts are depicted in Fig. 1. Before forming, the AA5182 aluminum blanks have been cleaned with acetone. The complete removal of the basic lubrication was verified with an oil sensor. The deep drawing of a 60 mm x 100 mm rectangular cup was performed with a hydraulic press (Lasco, TSP 100 So). Fig. 1 a) shows the resulting cup for 30 mm punch displacement and a normal pressure p_N in the flange area of 1.5 MPa. The

*E-mail address of corresponding author: jennifer.steiner@fau.de

cup reveals cracks in two corners but no wrinkles. Therefore, another test was derived with lower normal pressure to minimize the risk of cracks. However, even with a pressure of 0.3 MPa wrinkles and cracks occur which means that successful deep drawing is not possible (Fig. 1 b)). Thus, surface modifications need to be developed to decrease the friction and improve the material flow under dry conditions. Within the project 'Lubricant free forming with tailored tribological conditions' a tailored tool concept with locally adapted tribological conditions is designed. Based on elementary investigations about friction and wear of conventional surfaces under dry conditions, surface modifications in terms of coatings and laser generated micro features are currently qualified for the application in dry deep drawing operations.

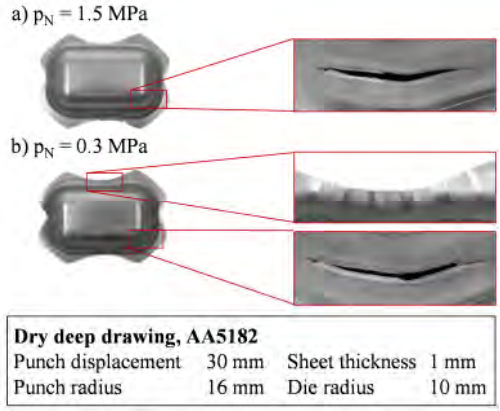

Fig. 1: Results of dry deep drawing with conventional tools

2 Methodology of investigation

The aim of this study is the evaluation of the tribological behavior of surface modifications developed for lubricant free sheet metal forming. The applied methodology of this investigation is depicted in Fig. 2.

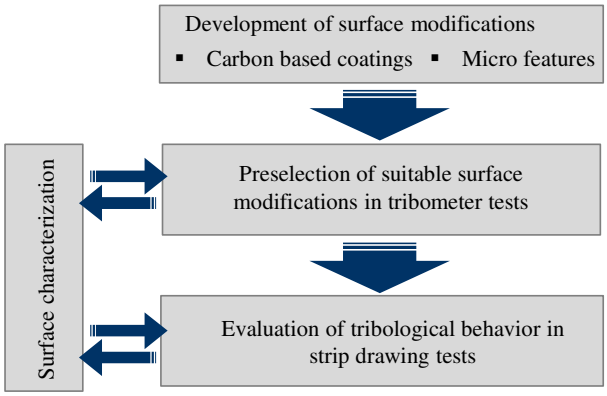

Fig. 2: Methodology for evaluation of surface modifications

First, the processes for deposition of carbon based coatings and laser texturing of micro features are investigated. Main purpose of coating application is decreasing adhesion tendency and friction. In contrast, micro features should locally increase friction of metallic bright and coated surfaces to control the material flow. By varying the process parameters the characteristics of the surface modifications are specifically adjusted to either reduce wear and friction with coatings or increase friction with patterned surfaces. In order to preselect promising types of modifications, a simple tribometer test setup as shown in 4.1 is used. Surface characterization is performed before and after testing to gain insights into the wear behavior. Afterwards, the tribological properties of certain surface modifications are evaluated in close to application strip drawing tests. Again, a tool and workpiece sided surface characterization is derived prior and after testing. As assessment criterions the determined friction coefficients as well as the surface quality and wear occurrence are taken into account.

As tool material the cold working steel X155CrVMo12 (1.2379) with a hardness of 60 ± 1 HRC was selected. A hardening process suitable for post coating deposition was chosen. The general surface finishing was achieved with a combined lapping and polishing process with oil based diamond suspension with a grain size of 9 µm. This procedure assures a smooth surface with an average peak to valley height of $R_z = 0.9 \pm 0.1$ µm and a reduced peak height of $R_{pk} = 0.10 \pm 0.01$ µm. As workpiece material the mild deep drawing steel DC04 and the aluminum alloys AA6014 and AA5182 with a sheet thickness of 1 mm and an electrical discharge texture (EDT) are examined. DC04 is commonly used in the automotive industry for inner and outer car body parts whereas the aluminum alloys are primarily used for add on units and hatches.

3 Development of surface modifications

3.1 Carbon based coatings

3.1.1 Sample preparation and characterization

The a-C:H:W and ta-C coating systems are deposited on ring-shaped tool steel substrates with inner and outer diameter of 10 mm and 20 mm. The rings are ultra-sonically cleaned in acetone and isopropanol. Prior to the deposition process the substrates are etched by bombardment of argon ions in order to remove the contaminants and stored gas molecules as well as humidity on the surface.

After deposition of the coatings, the surfaces are analyzed by electron scanning microscopy (SEM). The average distance between the highest peak and lowest valley R_z and the reduced peak height R_{pk} values are characterized by tactile stylus measurements according to DIN EN ISO 4287 [3]. The adhesion strength of the coating to the substrate is measured qualitatively by the Rockwell C indentation method according to VDI 3198 [4]. Using an optical microscope, coating adhesion is classified into 6 levels with HF 1 for the best adhesion and HF 6 for the worst. The crater grinder method is applied to measure the coating thickness according to DIN EN 1071-2 [5]. Micro hardness of 15 points on different places of the coatings is determined by Vickers indentation with indentation force of 0.002 kp (≈0.02 N) according to DIN EN ISO 14577-1 [6].

3.1.2 The a-C:H:W coating system

a-C:H:W coatings are applied for forming tools and many other fields because of their good adhesion to the substrate due to lower residual stresses and brittleness

compared to pure a-C:H coatings [7]. In this paper, a PVD/PACVD coating machine is used to deposit the a-C:H:W coating system which consists of an adhesive layer of chromium and tungsten carbide and the functional layer of a-C:H:W. As coating methods the arc evaporation and magnetron sputtering are used for the Cr adhesive layer and WC interlayer, respectively. The a-C:H:W layer is deposited by magnetron sputtering of a WC target using mid-frequency power supply (40 kHz, pulse width 5 µs) in argon-acetylene atmosphere. The substrate bias voltage and the argon flow in the coating chamber are varied because these two parameters affect strongly the mechanical properties and thus the tribological behavior [7]. The deposition time is coordinated so that a total coating thickness of about 4 µm is achieved. All deposition processes are carried out at 100 °C. The parameter details are listed in Tab. 1.

Tab. 1: Deposition parameters of a-C:H:W variations

Sample ID	U_{bias} in V	ϕ(Ar) in sccm	$\phi(C_2H_2)$ in sccm	P_{target} in kW
C01	57	128	40	1.4
C02	57	232	40	1.4
C03	130	180	40	1.4
C04	203	128	40	1.4
C05	203	232	40	1.4

Fig. 3 (a) and (b) show SEM images of a representative a-C:H:W coated surface after deposition without mechanical post-treatment. Fig. 3 (a) depicts that surface asperities due to small particles are distributed on the surface which result from a large number of macro-particles (droplets) entrapped in the Cr adhesive layer. In addition, the columnar structure of the a-C:H:W layer results in growth of grain boundary which further increases the coating roughness. Observing the surface topography in Fig. 3 (b) in detail, fractal geometry with repeated structure of micro grains is detected. Fig. 3 (c) shows a LSM (Laser Scanning Microscope) top view and Fig. 3 (d) depicts the height of surface asperities. They reveal the same surface structure as in the SEM pictures with particles distributed on the entire surface.

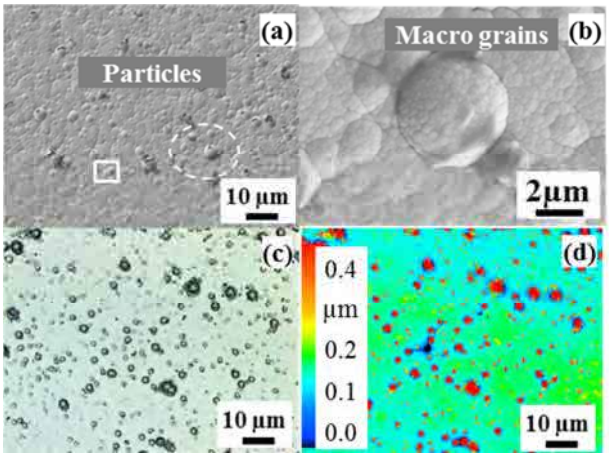

Fig. 3: SEM images of (a) particles and (b) macro grains of the a-C:H:W coating as well as LSM images of (c) coating surface and (d) topographic information

The average total thicknesses of the generated coatings are in the range of 4.1 µm to 5.9 µm. The roughness of the coated samples varies from R_z = 1.6 µm-2.0 µm and R_{pk} = 0.43 µm-0.66 µm which is two times higher for R_z und four times higher for R_{pk} values compared to uncoated substrates (Tab. 2).

Tab. 2: (a) Thickness and (b) roughness of a-C:H:W variants (n = 3)

	U_{bias} in V	ϕ(Ar) in sccm	t in µm	R_z in µm	R_{pk} in µm
C01	57	128	5.52 ± 0.55	1.85 ± 0.10	0.49 ± 0.03
C02	57	232	5.15 ± 0.09	1.88 ± 0.15	0.45 ± 0.04
C03	130	180	5.92 ± 0.64	1.64 ± 0.21	0.45 ± 0.06
C04	203	128	4.12 ± 0.40	1.62 ± 0.07	0.66 ± 0.04
C05	203	232	5.75 ± 0.61	2.00 ± 0.13	0.52 ± 0.06

The adhesion strength of the coatings C01 to C03 is between HF 3 to HF 4 which is acceptable as a functional layer. The coatings C04 and C05 are evaluated as HF 5 to HF 6. The reason for the poor adhesion of C04 and C05 might be the higher substrate bias voltage during the deposition process. Since the higher bias voltage causes higher residual stress and lattice distortion [8] which affects coating adhesion to the substrate.

In order to measure the hardness precisely, the same coating variants were deposited on the polished steel substrate (R_a = 0.02 µm, R_z = 0.19 µm) and the coated samples were also polished after deposition to $R_a \leq 0.02$ µm and $R_z \leq 0.2$ µm to ensure a smooth surface for indentation. The samples exhibit various *HM* at 20 mN from 2.4 to 3.7 GPa, elastic indentation modulus E_{IT} from 55.9 to 76.2 GPa and Vickers hardness *HV* from 415.8 to 652.5 (Tab. 3). The samples deposited at higher bias voltage such as C04 and C05 exhibit higher hardness and elastic indentation modulus. These coatings are dense and less porous compared to the ones deposited under lower bias [9]. In addition, the measured hardness values of the a-C:H:W variants here are lower compared to the a-C:H:W coatings with 2 µm in [10] and with 3 µm thickness in [11]. This mainly results from increased thickness. Intending the extension of durability of forming tool coatings, coating thickness is increased to 4 µm. The reason for this is that the relaxation of the atoms towards the top coating layer is stronger than towards the bottom layer. Consequently, a coating system with lower hardness on top and probably higher hardness on the bottom is generated.

Tab. 3: Martens hardness *HM 0.002*, indentation modulus E_{IT} *0.002* and Vickers hardness *HV 0.002* of a-C:H:W samples (n = 3)

Sample ID	*HM 0.002*. in GPa	E_{IT} *0.002* in GPa	*HV 0.002*
C01	2.9 ± 0.3	55.9 ± 2.8	528.9 ± 77.6
C02	2.4 ± 0.2	47.7 ± 2.4	415.8 ± 50.7
C03	2.8 ± 0.4	58.4 ± 5.0	473.1 ± 89.5
C04	3.7 ± 0.4	76.2 ± 5.0	652.5 ± 84.8
C05	3.4 ± 0.4	65.9 ± 5.2	612.1 ± 84.0
substrate	6.1 ± 0.4	209.1 ± 9.0	816.8 ± 58.4

3.1.3 The ta-C coating system

The ta-C coating system is deposited on the substrate with polished surface of $R_z = 0.16 \pm 0.01$ µm and $R_{pk} = 0.03 \pm 0.01$ µm. The ta-C coating system consists of an adhesive layer of Cr and the ta-C functional layer. For a smooth coating surface the Cr adhesive layer is generated by sputtering. The ta-C coating was manufactured by the laser arc process. The arc process is initiated by a laser pulse on the carbon (graphite) target [12]. In order to ensure a smooth coating, a magnetic field is used to filter the macro particles from the arc process. After the deposition the coated samples are mechanically treated by polishing and brushing with diamond paste with a grain size of 3 µm. ta-C surface was measured by laser scanning microscope (LSM) to evaluate its topography. Fig. 4 shows the ta-C surface after mechanical post-treatment. The surface reveals a typical polished structure with some valleys and peaks. Due to its high fraction of diamond-like carbon bonds (sp^3-bonds) the ta-C coating exhibit extremely high hardness and wear resistance [13]. The total coating thickness of the ta-C coating system is 1.33 µm. The roughness after surface finishing is $R_z = 0.26 \pm 0.01$ µm and $R_{pk} = 0.045 \pm 0.005$ µm. The coating exhibit a Martens hardness of $HM = 17.7$ GPa and a Vickers hardness of 4650 HV 0.002. The adhesion between coating and substrate is HF 2.

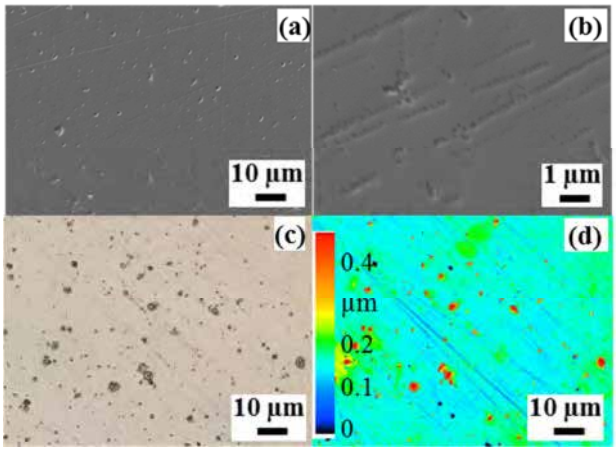

Fig. 4: SEM images of (a) ta-C surface and (b) grinding pattern on the surface as well as LSM images of (c) ta-C surface and (d) topographic information

3.2 Laser generated micro features

In order to control the material flow in the deep drawing process, laser generated micro features are applied on the coated ring surfaces. Because of its tribological performance a-C:H:W coating C03 is chosen for deposition (chapter 5.1). The laser based texturing step follows the coating process. After coating deposition and prior to laser processing the rings were polished to reduce the surface roughness to the initial level of the substrate. As the micro features have a depth $d_F = 20$ µm and the top layer is about 5 µm thick, the coating as well as parts of the substrate material are penetrated (Fig. 5). Feature depth is chosen to enable proper trapping of wear debris. Constant feature shape is set to be rectangular with width $b_F = 500$ µm and length $l_F = 200$ µm (Fig. 5).

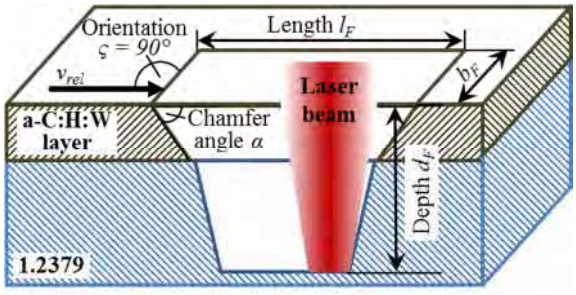

Fig. 5: Schematic isometric view of rectangular micro feature including the definition of feature properties

These dimensions are chosen to enable proper remove of wear debris from the contact area as well as the adjustment of the chamfer angle by laser texturing using a Gaussian intensity profile. At rotational sliding this shape ensures constant feature orientation and area coverage on each surface section.

Micro features are generated by ultrashort pulsed laser texturing with the laser system Fuego (Time-Bandwidth Products). The laser beam with a Gaussian intensity profile is deflected on the ring surface by means of the galvanometer scanner hurryScan II 14 (Scanlab). The spot diameter at the beam waist amounts to 32 µm. For texturing different parameter settings characterized by the peak fluence, the spot diameter, the hatch distance and the number of passes are applied (Tab. 4). The different peak fluences of these settings enable material removal of minimal burr at the feature edges on top of the surface. The combination of spot diameter, hatch distance and number of passes is set to adjust the chamfer angle under the constraint of constant feature depth $d_F = 20$ µm. Different chamfer angles $\alpha_A = 45°$ and $\alpha_B = 5°$ are generated by the variants A and B.

Tab. 4: Parameter settings of successive laser texturing steps for micro feature generation with high (A.1-3) and low chamfer angle (B.1-2)

Step No.	Peak fluence F_0 in J/cm²	Spot diameter d in µm	Hatch distance p_y in µm	Number of passes N
A.1	5.0	32	15	1
A.2	3.7	32	15	15
A.3	0.8	32	2	2
B.1	2.0	60	30	1
B.2	3.7	32	15	15

First, removal of the a-C:H:W layer is done by step A.1 or B.1. Second, 1.2379 is textured by A.2 or B.2. The high chamfer angle α_A of the micro feature (Fig. 5) is optionally realized by A.3. The scan speed of each setting is $v_S = 68$ mm/s. Different chamfer angles in the top layer and in the substrate material result from different parameters for removal of a-C:H:W and 1.2379. Before and after laser processing the samples are cleaned in an ultrasonic bath with isopropanol.

4 Test setup of laboratory tests

To evaluate the tribological behavior of the surface modifications two different types of laboratory tests are applied. For a first analysis of the modifications the ring-on-disc tribometer setup is used. Afterwards selected surfaces are investigated under conditions closer to forming processes in the flat strip drawing test. All experiments are performed under lubricant free conditions.

4.1 Setup of ring-on-disc tribometer

For the ring-on-disc tests a tribometer TRM1000 (Wazau) is used. The tribological system consists of a unidirectional rotating ring and a fixed sheet metal disc (Fig. 6).

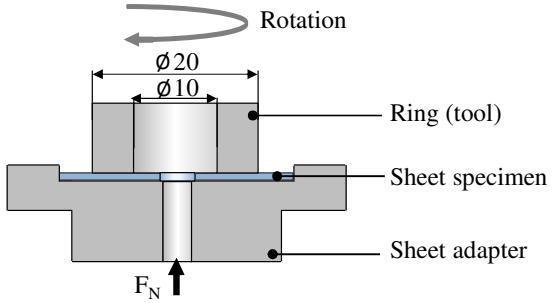

Fig. 6: Principle of the ring-on-disc tribometer

The chosen rotational speed v_U= 127 min^{-1} is equal to the usual speed of a punch in deep drawing of v_{rel}= 100 mm/s for the mean radius of the ring R_M= 7.5 mm. In the ring-on-disc tests the normal force F_N = 500 N is applied to adjust the normal pressure p_N = 2.1 MPa. For each ring-disc pairing the total sliding distance is set to s_{tot} = 10 m. This distance is about two orders of magnitude higher than sliding distance in conventional deep drawing operations. Thus, investigations on wear are enabled under the constraint of a closed tribological system. The sample size of every experimental condition is n = 3.

4.2 Setup of flat strip drawing test

The tribological system of the flat strip drawing test is characterized by a double sided contact with sliding friction. This conditions mirror the tribological loads in the flange area of deep drawing processes [14]. The used test setup is depicted in Fig. 7. The specimen is located between two friction jaws and is clamped on one side. To apply the defined normal force F_N the lower friction jaw moves upwards. The friction jaws have a contact area of 100 mm length and 55 mm width. The strips are wider than the tools to prevent a negative impact of the sheets cutting edges.

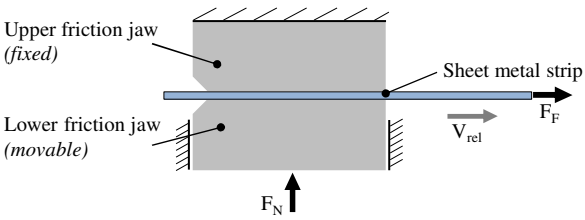

Fig. 7: Setup of flat strip drawing test

The recorded drawing force equals the cumulative friction force F_F between the sheet metal strip and the friction jaws. The friction coefficient μ is determined according to Coulomb's friction law in eq. (1).

$$\mu = (F_F / 2) / F_N \quad (1)$$

In order to investigate the steady state along the 190 mm total drawing length the evaluation area is defined between 100 mm and 170 mm. Thus, influences of starting and slowing down of the drawing cylinder are excluded.

5 Preselection of surface modifications

5.1 Tribological behavior of coated tools

Main goal of the tool surface coatings is the reduction of friction and adhesion in dry sliding with steel and aluminum sheets. In a first step, friction and wear behavior of tool sided coatings is evaluated in comparison to uncoated tools in ring-on-disc tests.

5.1.1 Friction

As shown in Fig. 8, friction coefficients μ_{rod} of a-C:H:W variants against DC04 measured with the ring-on-disc tribometer are in the range 0.52 to 0.90. The variant C03 shows lower μ_{rod} compared to the uncoated steel, while C02 is not significantly lower than the level of the reference. Both variants are deposited at a medium to high argon flow. It is assumed, that these variants have therefore a lower WC content [15], which leads to less adhesion of Zn or Fe due to lower metallic affinity. In addition, the slightly lower R_{pk} values of variants C02 and C03 cause slightly lower friction. The adhesion of the sheet material on the ring surface causes galling during sliding which leads to sticking and thus higher μ_{rod}.

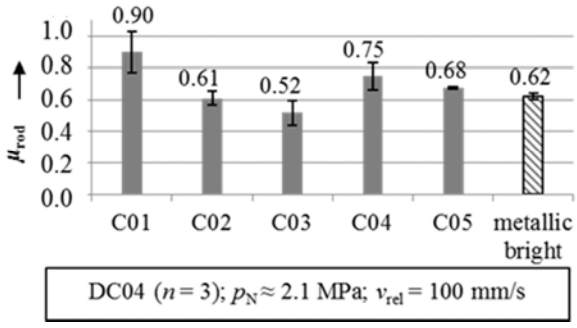

Fig. 8: Average friction coefficient μ_{rod} of a-C:H:W variants without post-treatment against DC04 for sliding distance of 2.5 to 10 m

In order to investigate the effect of coating roughness on the tribological behavior, variant C03 is selected and polished to surface roughness R_z = 0.54 ± 0.04 µm and R_{pk} = 0.06 ± 0.004 µm. As further constraints are constant, average friction coefficient of polished coating surfaces is reduced by 33 % due to post-treatment of the coating (Fig. 9).

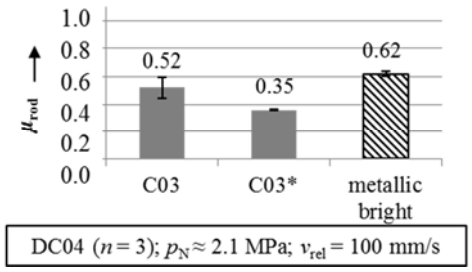

Fig. 9: Average friction coefficient μ_{rod} of a-C:H:W C03 without post-treatment, C03* with post-treatment and uncoated rings against DC04 for sliding distance of 2.5 to 10 m

To select suitable coating receipt for the strip drawing test with aluminum alloys, the a-C:H:W coating variants are tested exemplarily against AA6014. The average friction coefficients are in the range of 0.55 to 0.64, as shown in Fig. 10. The friction was almost not affected by different coating variants. Aluminum strongly adheres to a-C:H:W coatings. The reason for this general very high adhesion might be the WC content in the a-C:H:W coatings due to higher metallic affinity compared to the other carbon coatings without metallic dopant, such as the ta-C coatings. Thus, formation of direct contact between the aluminum sheet and adherent aluminum lead to similar μ_{rod}. The adhering sheet material prevents the direct contact between aluminum sheet and the actual coating surface.

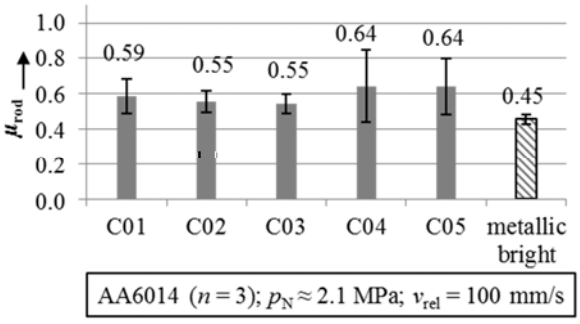

Fig. 10: Average friction coefficient μ_{rod} of a-C:H:W variants without post-treatment against AA6014 for sliding distance of 2.5 to 10 m

Additionally, the ta-C coating system is tested in the ring-on-disc tribometer. A reference test with metallic bright 1.2379, which was polished to the same R_{pk} value as the ta-C coating, is performed to eliminate the influence of varying surface roughness. The friction coefficients μ_{rod} in contact with the three sheet materials under dry conditions are shown in the Fig. 11.

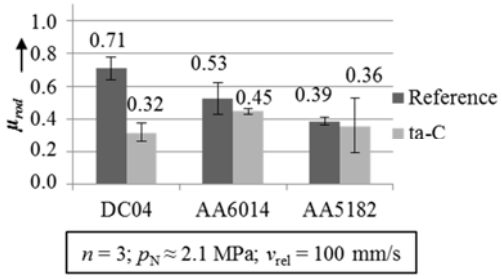

Fig. 11: Friction coefficient μ_{rod} of the ta-C coating against DC04, AA6014 and AA5182 for sliding distance of 2.5 to 10 m

During sliding against DC04 sheet, loose wear particles between the sheet and counter body are generated but the extremely hard coating protected the tool surface against scratching by these loose particles which results in a much lower μ_{rod} than that of a-C:H:W coating variants. Against the aluminum alloys the lower adhesion tendency of ta-C to metal contributes to a lower μ_{rod} compared to metallic bright tool surface.

5.1.2 Wear

Fig. 12 shows the wear tracks on the tested ring surfaces. The reference tests with metallic bright rings contacting DC04 and AA6014 show strong adherence from sheet materials. The a-C:H:W coated ring shows inhibitory effect against adhesion from DC04. After 1 m sliding distance only slight metal adhesion was observed on the coated surface. However, the a-C:H:W coated ring surface in contact with AA6014 shows large area of aluminum adhesion. In contrast, almost no or little adhesion from sheet material is observed on the ta-C coated rings.

Fig. 12: The wear tracks on tested rings against (a) DC04 and (b) AA6014

As shown in Fig. 13 (a), the smoothed area of the a-C:H:W variant C03 ring against DC04 is observed by SEM. Sliding tracks can be seen in this area. Fig. 13 (b) provides a cross view under this smoothed area by FIB (focused ion beam) cutting. The coating with a thickness of about 2.8 µm to 3.4 µm remains on the substrate, since the coating on top has been rubbed during the sliding process through abrasion.

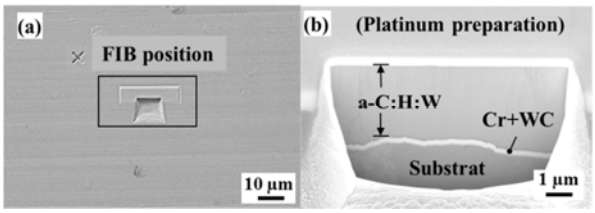

Fig. 13: SEM images of (a) the smoothed area of the tested a-C:H:W ring with the coating receipt C03 against DC04 and (b) FIB cross section in this area

The tested a-C:H:W rings against aluminum sheet AA6014 are generally covered by severe aluminum adhesions. After 1.5 m sliding distance, extensive aluminum adhesions on the coating surface were detected. After 3 m adhesive material covers the entire

ring surface. As shown in Fig. 14, the roughness tips distributed on the original a-C:H:W surface are the trigger for the aluminum adhesion.

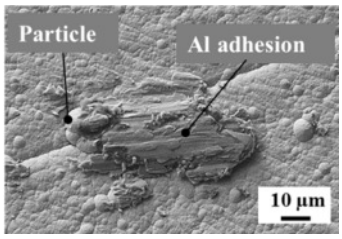

Fig. 14: SEM image of the primary aluminum adhesion caught by a roughness tip

A FIB cut is performed under the aluminum adhesion as shown in Fig. 15 (a). It can be seen in the cross section in Fig. 15 (b) that the coating surface is completely covered by aluminum and thus the whole coating system remained in its original condition after tribometer test.

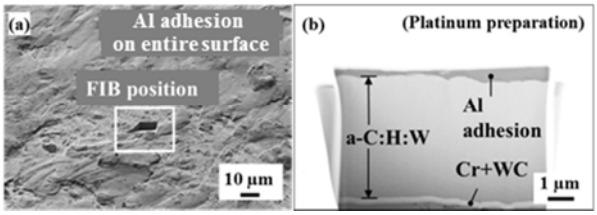

Fig. 15: SEM images of (a) the tested a-C:H:W ring covered by aluminum and (b) FIB cross section in this area

Compared to the a-C:H:W coating system, for the ta-C coated tools there are almost no Zn/Fe adhesions visible and only small-scale aluminum adhesions are observed. The reasons are on the one hand the mechanically fine polished surface; on the other hand, the lower tendency of adherence of the dopant-free carbon based coatings to aluminum alloys [16]. Fig. 16 shows the SEM image and the FIB cross sections of tested ta-C surface against AA6014 where aluminum adhered. The aluminum adhesions at this position are about 250 to 800 nm thick.

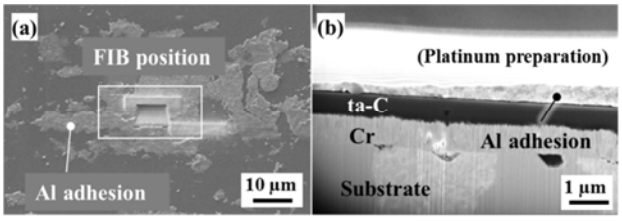

Fig. 16: SEM images of (a) the tested ta-C ring against AA6014 and (b) FIB cross section in this area

5.2 Tribological behavior of micro features

Adjustment and control of friction coefficient and material flow by micro features require the avoidance of sheet surface damage. Due to micro features plastic deformation of sheet sided asperities should be influenced. The tribological behavior of coated and patterned ring surfaces sliding on zinc-coated DC04 sheets is investigated because this sheet material has shown lower adhesion affinity than aluminum [10]. In ball-on disc tribometer tests Petterson et al. found out, that the orientation of 20 µm wide grooves on DLC coated sheets influences the friction coefficient and the wear of a steel ball [17]. As the ball material is even harder than the investigated zinc coating on DC04, the geometry of feature edges is expected to significantly affect tribological behavior. Therefore, the influences of the area coverage respectively the number of feature edges, the edge orientation and the chamfer angle of the micro features are investigated for the material pairing a-C:H:W (C03)/DC04 (Tab. 5). Feature properties are chosen to cause a maximum difference of evaluated friction coefficient and wear.

Tab. 5: Properties of rectangular micro features on DLC coated ring surface investigated in ring-on-disc tribometer tests

Test	Area coverage δ_F in %	Chamfer angle α in °	Orientation ζ in °
Ref.		Non-patterned	
P1	50	45	90
P2	50	5	90
P3	10	5	90
P4	10	5	45

5.2.1 Friction

For comparison and reference purposes a-C:H:W coated non-patterned rings are tested. The mean friction coefficient μ_{rod} of these samples shows a constant trend (Fig. 17). The μ_{rod} average of the reference is significantly below the before mentioned $\mu_{rod} = 0.59$ of the metallic bright non-patterned reference (chapter 5.1.1) due to lower $R_{pk} = 0.11 \pm 0.04$ µm compared to $R_{pk} = 0.45 \pm 0.06$ µm. This roughness is realized by additional post-polishing. Each of the tested patterned surfaces P1 - P4 shows higher μ_{rod} than the non-patterned ring. The higher tested area coverage $\delta_F = 50$ % together with the higher chamfer angle $\alpha = 45°$ shows the most unstable trend of μ_{rod} (P1). At sliding distance $s < 2.0$ m smoothening of the contact surfaces occur (regime R-I, Fig. 17). At sliding distances $s > 2.0$ μ_{rod} strongly increases due to shearing of zinc at the feature edges (regime R-II, Fig. 17) which is visible by scratches on exemplary proven disc after $s = 1.5$ m. This shearing is influenced by the number and geometry of the edges. The strong fluctuation of μ_{rod} at longer sliding distances (regime R-III, Fig. 17) is explained by adhesion between zinc particles trapped in the micro features and the zinc layer on the disc [10].

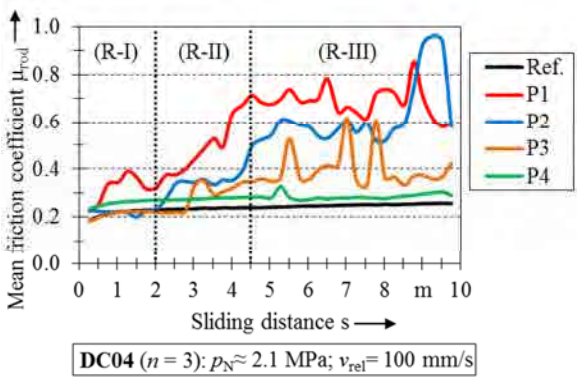

Fig. 17: Trend of mean friction coefficient μ_{rod} depending on the sliding distance for the non-patterned reference (Ref.) and patterned rings (P1-4) in different regimes of sliding R-I (0.5-2.0 m), R-II (2.0-4.5 m) and R-III (4.5-10 m)

Compared to test P1 the lower chamfer angle α = 5° leads to lower level of μ_{rod} for $s < 2.0$ m where smoothening of the surfaces occur. Afterwards, zinc is sheared at the feature edges, which leads to rising and fluctuating μ_{rod} (Tab. 6). The reduction of the number of feature edges by decreasing the area coverage in test P3 causes even a longer sliding distance of smoothening compared to P2 because μ_{rod} begins to rise at $s \approx 2.6$ m. But zinc abrasion and thus galling of trapped zinc particles still cannot be avoided by this feature setting.

Tab. 6: Friction coefficients μ_{rod} within different regimes of R-I (0.3 - 2.0 m), R-II (2.0-4.5 m) and R-III (4.5-10 m) ($n = 3$)

	R-I	R-II	R-III
Ref.	0.22 ± 0.01	0.24 ± 0.01	0.25 ± 0.01
P1	0.33 ± 0.04	0.48 ± 0.12	0.67 ± 0.09
P2	0.22 ± 0.01	0.35 ± 0.07	0.62 ± 0.17
P3	0.21 ± 0.01	0.29 ± 0.06	0.40 ± 0.12
P4	0.26 ± 0.01	0.28 ± 0.01	0.28 ± 0.02

Regarding a stable trend of mean friction coefficient, a significant decrease of zinc shearing is achieved by an additional change of the feature orientation in test P4. The regime of smoothening is significantly extended. The mean value of P4 $\mu_{rod} = 0.28 \pm 0.02$ is higher than for the coated non-patterned reference $\mu_{rod} = 0.24 \pm 0.01$ and hence is appropriate for the desired friction increase (Fig. 18).

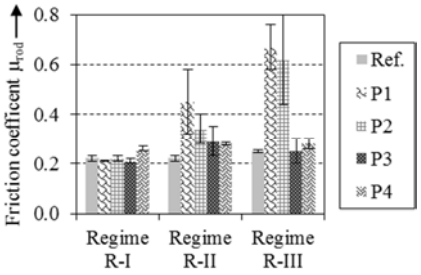

Fig. 18: Friction coefficients μ_{rod} within different regimes of smoothening R-I (running-in, 0.3-2.0 m), transitional regime R-II (2.0-4.5 m) and stationary sliding R-III (4.5-10 m) ($n = 3$)

5.2.2 Wear

Similar to the trend of friction coefficient micro feature properties affect wear of the ring and surface quality of the disc. The discs tested on non-patterned reference rings show a homogenous sliding track where the asperities are reduced due to plastic deformation during the phase of smoothening (Fig. 19 a)). Local removal of the zinc layer followed by local galling of zinc on the disc occurs. Galling is caused by zinc particles in the contact zone and is observable by a local height increase on the disc [18]. This unwanted decrease of disc surface quality should be avoided by fast detachment of particles out of the contact zone e.g. by micro features. As a consequence of galling zinc residues are found on the ring surface (Fig. 19 b)). The slightly shining ring surface at the outer edge indicates smoothed asperities in this area. Due to local contact of partial uncovered DC04 and a-C:H:W, abrasion occurs and leads to a local removal of 1 µm a-C:H:W-layer at the investigated sliding distance $s_{tot} = 10$ m.

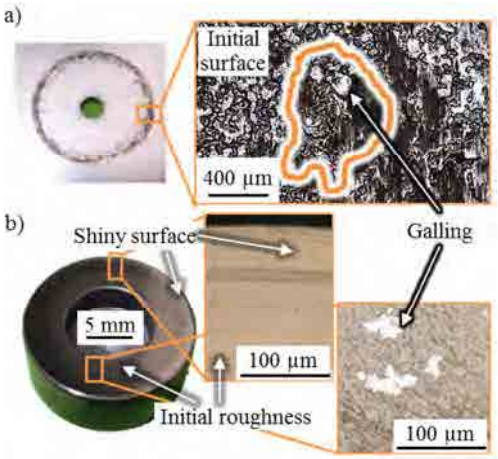

Fig. 19: Tested reference samples: a) Sliding track on the disc inclusive zinc galling, b) ring surface with shiny surface at the outer edge due to smoothening and zinc particles on the surface

The feature properties of test P1 cause distinct abrasion of zinc. The zinc particles are trapped by the micro features which results in 51 ± 15 % filling degree of completely available feature volume. This filling degree is exemplarily measured once on each ring in the region of interest (ROI) and represents the highest one of the tested patterned samples P1 - P4 (Fig. 20 a)). The ROI is depicted in [10] and encloses an area which corresponds to the triple feature length times the ring radius.

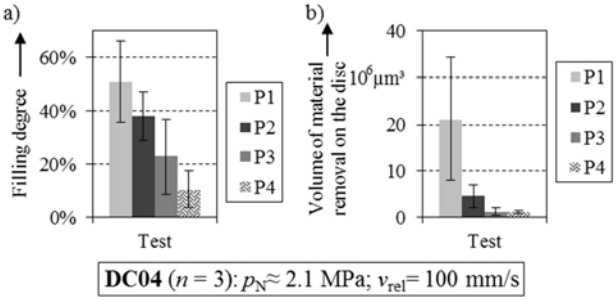

Fig. 20: a) Filling degree of micro features and b) volume of material removal of the disc surface measured in the ROI

Strong abrasion of zinc leads to local uncovered DC04 discs. The resulting partial DLC/DC04 contact induces abrasion of the a-C:H:W-layer and can be observed by micro scratches. These micro scratches start between the features and end at the feature edges where the particles are trapped (Fig. 21 a)). The lower chamfer angle $\alpha = 5°$ - hence less sharp edges - in test P2 induces less zinc particle volume characterized by the filling degree and compared to P1 (Fig. 20 a)). But the zinc removal at the disc is still too high (Fig. 20 b)) regarding sufficient disc surface quality. The zinc removal is measured once on each disc in a ROI with same dimensions as on the ring and represents the volume below the level of valleys of EDT texture. The removal of the disc can be significantly reduced by a decrease of the number of feature edges in test P3. Thus, less zinc particles are trapped which results in lower filling degree compared to P2 (Fig. 20 a)). Although the existing total feature volume of test P3 is only one fifth of P2 the filling degree is about 20 %. Therefore, the

area coverage $\delta_F = 10\%$ reduces abrasion, but shearing at single edges is again too high to avoid any unwanted disc damage. The necessary further reduction of zinc removal is achieved by the systematic decrease of the three-dimensional chamfer angle which is influenced by the chamfer angle and the orientation. For this, the feature orientation is changed towards $\zeta = 45°$ and the chamfer angle stays constant at $\alpha = 5°$. This low chamfer angle together with the orientation affects constant friction coefficient as well as zinc removal from the disc. Zinc abrasion slightly exists but is significantly reduced and leads to lower filling degree of the features below 20 %. Galling is completely avoided and the a-C:H:W layer on the ring is only smoothed at the outer edge (Fig. 21 b)).

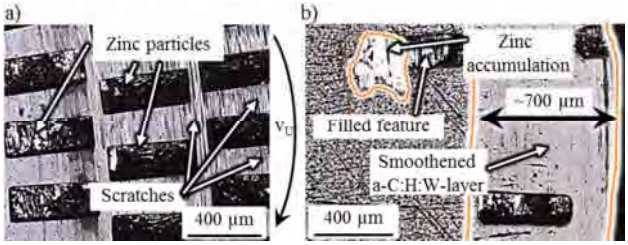

Fig. 21: Ring surface of test a) P1 with worn a-C:H:W-layer and b) P4 with only smoothed surface at the outer edge after s_{tot} = 10 m

Summarizing the effects of the feature properties on friction and wear, it can be stated that abrasion is strongly influenced by the chamfer geometry characterized by its angle and orientation as well as the number of feature edges. Sharp edges respectively high chamfer angles induce abrasion of zinc even at short sliding distances below 2 m in the ring-on-disc tribometer. Low chamfer angles and the orientation $\zeta = 45°$ enable continuous smoothening of disc asperities. Adhesion of zinc resulting from zinc abrasion can be avoided. The variation of the number of feature edges e.g. by varying the area coverage enables the adjustment of friction increase as well as abrasive wear.

6 Tribological behavior of selected surface modifications in strip drawing tests

Additionally, strip drawing tests are performed in order to evaluate the tribological behavior of surface modifications under conditions close to a deep drawing process. Tab. 7 summarizes the testing parameters. For each sheet material a reference test under dry conditions in contact with a metallic bright jaw is conducted. DC04 would require higher contact pressure in the flange area than aluminum alloys. Thus, for DC04 a higher pressure level of 4.5 MPa compared to 1.5 MPa for AA6014 and AA5182 was selected for strip drawing tests. The a-C:H:W coating C03 was selected for further investigation because this variant showed the best tribological behavior in the tribometer tests. For an a-C:H:W (C03) coated ring surface without post treatment an average friction coefficient μ_{rod} of 0.52 was achieved in contact with DC04. In comparison, a much lower μ_{rod} of 0.35 resulted according to ring-on-disc tests with a-C:H:W (C03) rings which were polished after coating deposition. Therefore, all a-C:H:W coated jaws were polished after the coating process until the initial roughness level of R_{pk} = 0.1 µm was accomplished. Furthermore, the ta-C coating system described in chapter 3.1.3 was applied on the friction jaws. To analyze the influence of laser generated micro features in an open tribosystem metallic bright jaws were structured. The micro features have a depth of 5 µm, a width b_F = 500 µm and length l_F = 100 µm. Reason for lower depth and length compared to the features investigated in the ring-on-disc test is the much shorter sliding distance in the strip drawing test. Because of this smaller distance less wear particles are expected which means that a lower feature volume is sufficient. The area coverage was set to 10 % of the contact area because this level of coverage showed the best wear behavior in the above mentioned tribometer tests. The chamfer angle was set to $\alpha = 16°$ and the features were generated in orientation of $\zeta = 90°$. For each investigated tool surface (metallic bright, a-C:H:W coated, ta-C coated and metallic bright/ patterned) one pair of friction jaws was manufactured for each sheet material.

Tab. 7: Experimental design of strip drawing tests

v_{rel} in mm/s		100			
m_{dry} in g/m²		0.0			
Sheet material	p_N in MPa	Friction jaw surfaces			
		bright	a-C:H:W (C03)	ta-C	patterned (bright)
DC04	4.5	x	x	x	x
AA6014	1.5	x	x	x	x
AA5182	1.5	x	x	x	x

6.1 Determination of friction coefficients

The resulting friction coefficients for the test series with DC04 are summarized in Fig. 22. Even under dry conditions a relatively low friction is determined independently from the tool surface. The values for µ vary between 0.14 and 0.15. The deposited a-C:H:W and ta-C coatings could not achieve a reduction of the friction coefficient under the investigated load conditions. However, they might have a positive influence on the wear resistance of the tool.

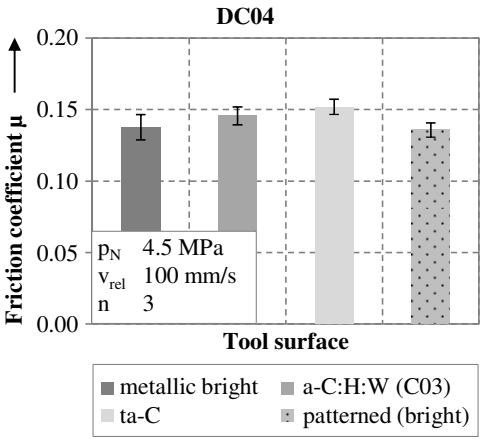

Fig. 22: Friction coefficients for DC04 in contact with varying tool surfaces under dry conditions

Fig. 23 depicts the influence of surface modifications on the friction coefficients in contact with

AA6014. Under dry conditions with metallic bright tools the friction coefficients exceed $\mu_{max} = 0.577$ according to the von Mises yield criterion. A friction coefficient above this level indicates local plastic deformation of sheet material. Applying coated friction jaws leads to a significant lower friction coefficient. Comparing the two coating types, a-C:H:W coated tools reveal still a high friction of 0.45 whereas ta-C coated jaws achieve a friction coefficient of 0.16. For the metallic bright, patterned tool surfaces the friction coefficient varies between 0.5 and 0.6. Thus, there is no significant difference in the tribological behavior between the metallic bright and the patterned surfaces.

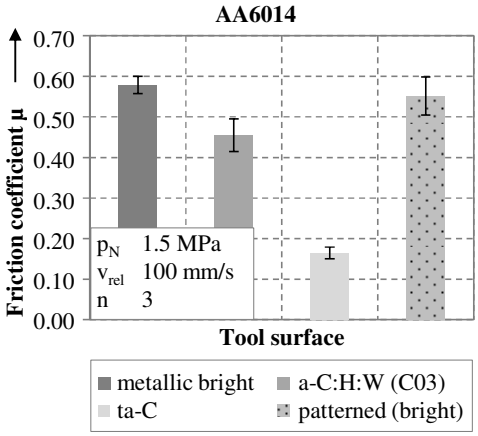

Fig. 23: Friction coefficients for AA6014 in contact with varying tool surfaces under dry conditions

The friction coefficients of AA5182 in contact with various tool sided modifications are given in Fig. 24. For a conventional tool surface the friction reaches a level of about 0.3. The a-C:H:W coated tools lead to an increasing friction coefficient up to 0.53. In contrast, ta-C coatings achieve a significant friction reduction compared to metallic bright and a-C:H:W coated tools. The friction coefficient of ta-C coated tools in contact with AA5182 varies between 0.15 and 0.16. Patterned tool surfaces cause an increase of friction from 0.3 to 0.49 compared to metallic bright surfaces.

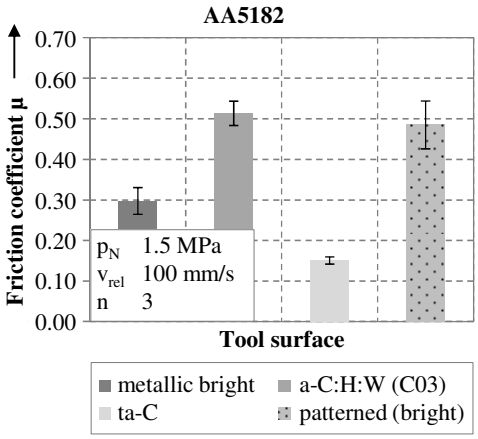

Fig. 24: Friction coefficients for AA5182 in contact with varying tool surfaces under dry conditions

The direct contact between tool and workpiece leads to a high influence of the sheet material on the tribological conditions. The anticorrosive zinc layer covering DC04 reveals a low adhesion tendency against tool steel which causes generally low friction coefficients under dry conditions. The zinc layer operates as kind of solid lubricant which leads to stable friction conditions independent of tool surface properties in terms of topography and chemistry. However, coatings could improve tool life and workpiece quality.

In contrast, aluminum alloys show a higher adhesion affinity towards tool steel when there is no separating lubrication film. This leads to intensive interaction in the contact area which causes higher friction coefficients. The tribological behavior of the investigated a-C:H:W coating depends on the contacting sheet material. For DC04 no significant influence on the friction coefficient occurs. Analyzing the results for AA6014 tests a slight reduction of the friction coefficient is achieved. In contrast, the experiments with AA5182 result in a distinctive increase of friction in contact with a-C:H:W. Comparing the results for ta-C coated friction jaws, an almost constant low level of friction is determined for all investigated sheet materials. The ta-C coated surfaces act as a separating layer between the workpiece and the tool steel. Thus, the tribological behavior of ta-C coatings is evaluated as a promising substitute of conventional lubricants. Looking at the results for the micro features, for DC04 and AA6014 no significant changes of friction are determined compared to non-patterned surfaces. However, for AA5182 a remarkable increase of friction is measured in contact with patterned tools. Regarding the laser generated micro features further investigations will be required to improve the understanding of their tribological influence. Within the overall scope of this research project, the main tasks of the micro features are to control the material flow by locally increasing friction and remove wear particles from the contact area. However, because of the high level of friction for metallic bright jaws in contact with aluminum alloys a coating of the forming tools will be essential. A locally increased friction coefficient might then be achieved with a coated and finally patterned surface like shown in chapter 5.2.1. To evaluate the possible range of increasing friction due to micro features, further experiments with a combination of coating and patterning are necessary.

6.2 Results of surface characterization

To get an overall impression of the tool surfaces after the strip drawing tests, photographs were taken of each combination of surface modification and sheet material. Additionally, confocal microscopy was used to qualitatively analyze the wear behavior. The results of the optical surface characterization are in good accordance with the determined friction coefficients. Fig. 25 shows the friction jaw surfaces after the tests with DC04 strips. The metallic bright and coated surfaces reveal no visible sign of wear. Only the patterned jaws depict a small amount of zinc particles adhering on the edge of micro features. The tool surfaces reveal no significant changes of the surface properties which indicate less intensive interaction with

the sheet material. This might be a reason for the relatively low and stable friction coefficients for DC04.

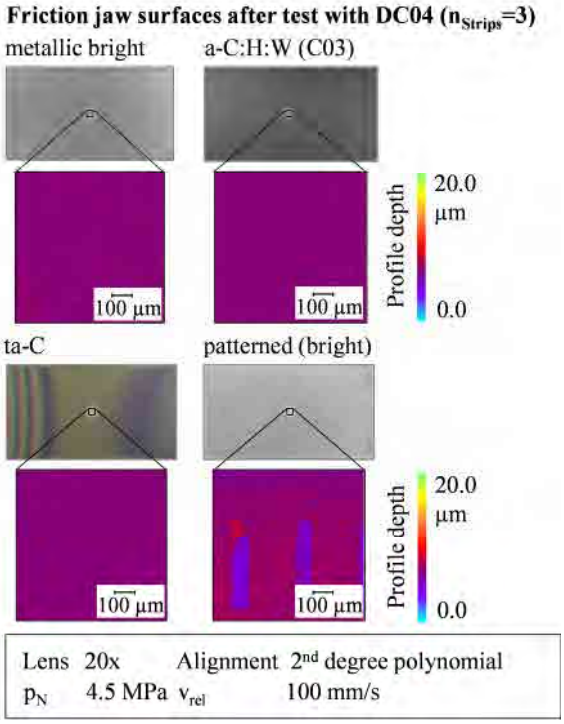

Fig. 25: Friction jaw surfaces with varying surface modifications after strip drawing tests in contact with DC04

Majority of tool surfaces show severe wear for the contact with AA6014 as depicted in Fig 26. Strong adhesion of sheet material reveals on the metallic bright and the a-C:H:W coated surfaces. The height of the adhesion reaches nearly 20 µm. Furthermore, the patterned surfaces show distinct adhesion of AA6014 on wide parts of the contact area.

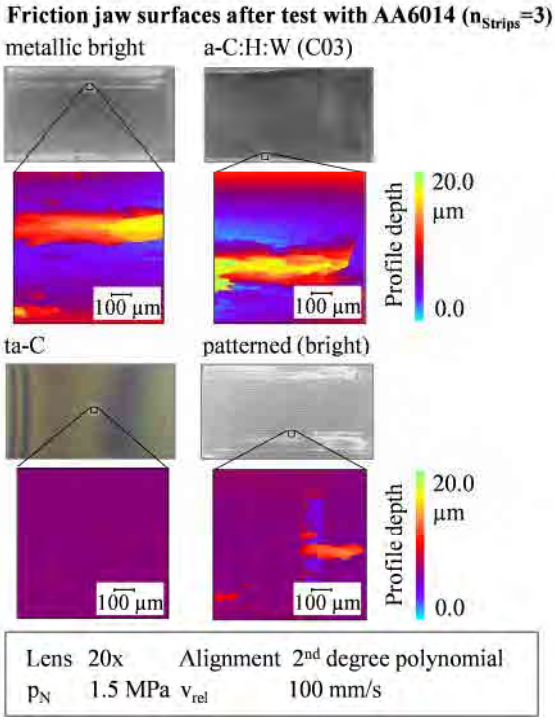

Fig. 26: Friction jaw surfaces with varying surface modifications after strip drawing tests in contact with AA6014

Solely the ta-C coated friction jaws display no measurable signs of wear under the investigated testing conditions. The amount of adhesion correlates with the level of friction coefficients. The highest friction and the strongest adhesion occur for the metallic bright and the patterned surfaces. A slightly lower friction and also less adhesion is determined for the a-C:H:W coated tools. Low friction coefficients and no assessable wear result with ta-C coated jaws.

In Fig. 27 the contact surfaces of metallic bright and modified jaws after the experiments with AA5182 are presented. The main remarkable wear mechanism is adhesion of sheet material on the tool steel. For metallic bright jaws only minor adhesion occurs in the middle of the contact area. A strong increase of the amount of adhesion reveals for a-C:H:W coatings. To analyze the reason for the increasing friction and adhesion the roughness of the jaws was characterized by tactile stylus measurements. Due to post treatment of the coated surface the a-C:H:W coated jaws reveal an even lower roughness than the metallic bright ones.

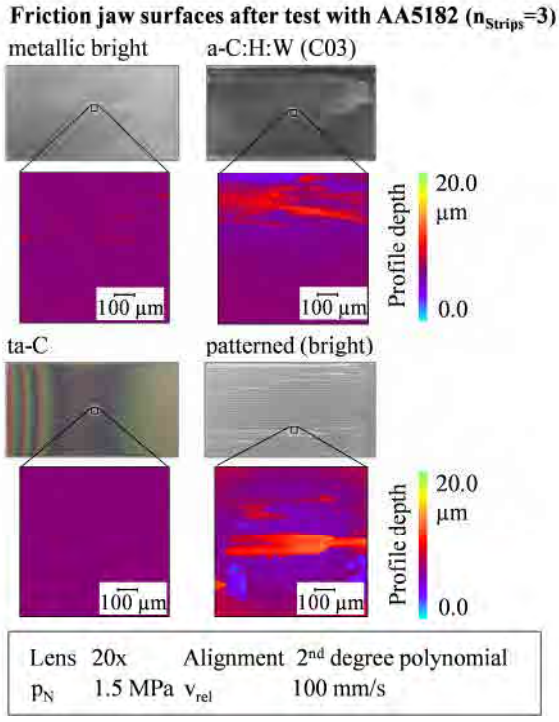

Fig. 27: Friction jaw surfaces with varying surface modifications after strip drawing tests in contact with AA5182

For example the peak to valley roughness R_z is reduced from 0.97 µm to 0.74 µm for the coated surface as well as the reduced peak height R_{pk} which decreased from 0.13 µm to 0.1 µm. Thus, the topographical changes due to the surface modifications seem not to be the reason for the distinctive worsening of the tribological behavior. Therefore, changed mechanical and chemical properties of the coated surfaces must be the reason for the increased tendency of adhesion. Further investigations are necessary to analyze which properties caused the insufficient tribological behavior. Comparing the metallic bright and the patterned jaws, a significantly higher amount of adhesion is visible on the tools with the laser generated micro features. This

intensive interaction with the sheet material explains the increase of friction coefficient for the patterned surfaces. Reason for increased wear might be sharp edges on the features – characterized by the chamfer angle $\alpha = 16\,°$ and the feature orientation $\zeta = 90°$ - which cause a stronger interlocking with the contacting asperities of the sheet material. Using ta-C coated tools in direct contact with AA5182 reveals no visible signs of wear. Once more the determined low friction coefficient correlates with the absence of adhesive wear mechanisms.

Analyzing the surface properties after the strip drawing tests provided insights into the wear behavior of the selected surface modifications. Main reason for wear occurrence is the strong adhesion tendency of the aluminum alloys. Under dry conditions, the amount of wear as well as the friction coefficient depends on the investigated sheet materials. Overall, the best tribological behavior in terms of low friction and no visible adhesion reveals for ta-C coated tools. Further investigations need to proof whether these coatings can resist also higher loads and longer sliding distances.

7 Discussion of tribological interactions

Basic trends regarding friction and wear behavior are similar for ring-on-disc and strip drawing test. However, the level of friction coefficient and wear volume is different for closed and open tribological systems. Within both laboratory tests ta-C coatings prevent adhesion and reduce friction. In contrast, the deposition of a-C:H:W layers enabled slight friction reduction for DC04. Low coating roughness is essential to avoid arising adhesion in every case. Especially, in contact with aluminum alloys high friction and strong adhesion is observed. Even with post-treated friction jaws a-C:H:W coatings could not prevent adhesion in strip drawing tests, too. Reason for the insufficient behavior might be the content of tungsten which has higher affinity towards aluminum than metallic-free coatings like ta-C. In addition, the surfaces of investigated ta-C coatings have a generally lower roughness which reduces the interlocking of asperities. The interlocking and smoothening affect the friction within tribosystems which are characterized by low adhesion affinity.

Smoothening is only slightly influenced by micro features due to interlocking of asperities at feature edges which is visible on the patterned tool topographies. At longer sliding distances within closed tribosystems the edge geometry influences abrasion of the smoother workpiece material. A smaller chamfer angle induces less abrasive wear particles. The defined feature volume is too small to remove all debris from the contact zone. Thus, some features are completely filled with particles and cause direct contact between sheet material and wear particles. This contact increases adhesion due to high bonding forces between same materials. In contrast, in open tribological systems mainly smoothening occurs due to the continuous supply with rough sheet material. Thus, the tested setting of low number of edges and comparatively low chamfer angle of the micro features induces low abrasion. Aiming for a significant increase of friction to control the material flow the number of edges should be increased without increasing abrasion.

8 Summary and Outlook

This paper presents effects of surface modifications on tribological behavior of lubricant free sliding. Forming of exemplarily drawn aluminum cups revealed that the application of conventional tooling concept is not suited for dry deep drawing.

Two types of carbon based coatings are investigated under dry conditions. Hydrogen-free ta-C coatings reveal a promising tribological behavior in open and closed tribosystems independent of contacting sheet material. In contrast, hydrogenous and tungsten doped a-C:H:W coatings reveal high friction and distinct adhesion in contact with aluminum alloys. Future investigations with a-C:H top layers will be performed to analyze whether the tungsten content is main reason for the poor tribological behavior. Additionally, the parameters of coating deposition will be varied to increase hardness and reduce roughness of the coated surfaces. a-C:H:W coatings will be further improved by doping with additional elements to decrease adhesion.

Aiming for a friction increase to control the material flow and achieving wear particle trapping, micro features on a-C:H:W coated rings are tribologically investigated. The development of determined friction coefficients showed that the number and geometry of the feature edges significantly influence interlocking of asperities. Therefore, abrasion and adhesion can be adjusted by variation of area coverage by micro features and their chamfer angle and orientation. Friction increase due to micro features is also observed on AA5182 in strip drawing tests. In further investigations coated as well as coated and patterned surfaces will be investigated at higher loads and longer sliding distances within the open tribosystem.

Acknowledgement

The authors thank the German Research Foundation (DFG) for supporting the presented investigations by funding the priority program SPP 1676 project ME 2043/43-1, SCHM 2115/36-1 and TR 1043/1-1 with the project title “Lubricant free forming with tailored tribological conditions”.

References

[1] N. Bay, A. Azushima, P. Groche, I. Ishibashi, M. Merklein, M. Morishita, T. Nakamura, S. Schmid, M. Yoshida: Environmentally benign tribo-systems for metal forming. CIRP Ann. Manuf. Techn. 59 (2) (2010) 760–780

[2] F. Vollertsen, F. Schmidt: Dry Metal Forming: Definition, Chances and Challenges. Int. J. Precision Engineering and Manufacturing – Green Technology 1/1 (2014) 59-62

[3] DIN 4287: Geometrische Produktspezifikation (GPS) - Oberflächenbeschaffenheit: Tastschnittverfahren - Benennungen, Definitionen und Kenngrößen der Oberflächenbeschaffenheit. Deutsches Institut für Normung e.V. (Hrsg.), Berlin: Beuth, 2010

[4] VDI 3198: Beschichten von Werkzeugen der Kaltmassivumformung: CVD- und PVD-Verfahren. Verein Deutscher Ingenieure (Hrsg.), Düsseldorf, 2004
[5] DIN 1071-2: Hochleistungskeramik - Verfahren zur Prüfung keramischer Schichten - Teil 2: Bestimmung der Schichtdicke mit dem Kalottenschleifverfahren. Deutsches Institut für Normung e.V. (Hrsg.), Berlin: Beuth, 2003
[6] DIN EN ISO 14577-1: Metallische Werkstoffe - Instrumentierte Eindringprüfung zur Bestimmung der Härte und anderer Werkstoffparameter - Teil 1: Prüfverfahren. Deutsches Institut für Normung e.V. (Hrsg.), Berlin: Beuth, 2003
[7] B. Vengudusamy, J.H. Green, G.D. Lamb, H.A. Spikes: Influence of hydrogen and tungsten concentration on the tribological properties of DLC/DLC contacts with ZDDP. Wear. 298-299 (2013) 109-119
[8] A.J. Perry, J.P. Schaffer, J. Brunner, W.D. Sproul.: A study of the picostructure of sputtered ZrN filmls. Surf. Coat. Tech. 49 (1991) 188-193
[9] Hetzner, H.; Zhao, R.; Tremmel, S.; Wartzack, S.: Tribological adjustment of tungsten-modified hydrogenated amorphous carbon coatings by adaption of the deposition parameters. In: Bouzakis, K.-D.; Bobzin, K.; Denkena, B. Merklein, M. (Hrsg.): 10th International Conference THE "A" Coatings, 10.-11. April 2013, Aachen: Shaker, S. 39-49.
[10] M. Merklein, M. Schmidt, S. Tremmel, S. Wartzack, K. Andreas, T. Häfner, R. Zhao, J. Steiner: Investigation of Tribological Systems for Dry Deep Drawing by Tailored Surfaces. Dry Met. Forming OAJ FMT 1 (2015) 57-62
[11] A. Banerji, S. Bhowmick, A.T. Alpas: High temperature tribological behavior of W containing diamond-like carbon (DLC) coating against titanium alloys. Surf. Coat. Tech. 241 (2014) 93-104
[12] T. Stucky, U. Baier, C.-F. Meyer, H.-J. Scheibe, B. Schultrich: Großflächenbeschichtung mit superhartem Kohlenstoff. Vak. Forsch. Prax. 15(6) (2003) 299-304
[13] Y. Mabuchi, T. Higuchi, V. Weihnacht: Effect of sp2/sp3 bonding ratio and nitrogen content on friction properties of hydrogen-free DLC coatings. Tribol. Int. 62 (2013) 130-140
[14] E. Doege, K.-P. Witthüser, R. Grahnert: Untersuchung der Reibungsverhältnisse beim Tiefziehen. In: Tribologie: Reibung, Verschleiß, Schmierung. Berlin: Springer, 1981.
[15] H. Hetzner: Systematische Entwicklung amorpher Kohlenstoffschichten unter Berücksichtigung der Anforderungen der Blechmassivumformung. Dissertation, University Erlangen-Nuremberg, 2014.
[16] W. Ni, Y. Cheng, A.M. Weiner, T.A. Perry: Tribological behavior of diamond-like-carbon (DLC) coatings against aluminum alloys at elevated temperatures. Surf. Coat. Tech. 201 (2006) 3229-3234
[17] U. Petterson, S. Jacobson: Influence of Surface Texture on Boundary Lubricated Sliding Contacts, Tribol. Int. 36 (2003) 857-864
[18] T. Häfner, J. Heberle, M. Dobler, M. Gränitz, I. Alexeev, M. Schmidt: Friction adjustment within dry deep drawing by locally laser textured tool surfaces. Key Eng. Mat. 639 (2015) 57-64